Mechanics of Materials 60 (2013) 159–170

Contents lists available at SciVerse ScienceDirect

Mechanics of Materials

journal homepage: www.elsevier.com/locate/mechmat

Fibrous composites of piezoelectric and piezomagnetic phases

Hsin-Yi Kuo [a], Kaushik Bhattacharya [b,*]

[a] Department of Civil Engineering, National Chiao Tung University, Hsinchu 30010, Taiwan
[b] Division of Engineering and Applied Science, California Institute of Technology, Pasadena, CA 91125, USA

ARTICLE INFO

Article history:
Received 23 March 2010
Received in revised form 18 October 2012
Available online 4 January 2013

Keywords:
Magnetoelectricity
Fibrous composite
Piezoelectric
Piezomagnetic

ABSTRACT

We propose a theoretical framework for evaluation of magnetoelectroelastic potentials in a fibrous composite with piezoelectric and piezomagnetic phases, motivated by the technological desire for materials with large magnetoelectric coupling. We show that the problem with transversely isotropic phases can be decomposed into two independent problems, plane strain with transverse electromagnetic fields and anti-plane shear with in-plane electromagnetic fields. We then consider the second problem in detail, and generalize the classic work of Lord Rayleigh (1892) to obtain the electrostatic potential in an ordered conductive composite and its extension to a disordered system by Kuo and Chen (2008) to the current coupled magnetoelectroelastic problem. We use this method to study $BaTiO_3$–$CoFe_2O_4$ composites and provide insights into obtaining large effective magnetoelectric coefficient.

1. Introduction

A variety of technological applications including magnetic field sensors, electrically controlled microwave devices and magneto-electric memory cells have motivated the study of magneto-electric coupling in materials and composites (Eerenstein et al., 2006; Nan et al., 2008). The magneto-electric coupling was predicted by Landau and Lifshitz (1984) and observed by Astrov (1960) and by Rado and Folen (1961) over fifty years ago. The coupling is weak in monolithic materials, and this has motivated the study of composites of piezoelectric and piezomagnetic media. The idea is that the applied electric field causes a deformation of the piezoelectric material which in turn induces a deformation in the piezomagnetic material thereby inducing a magnetic field.

The performance of a piezomagnetic/piezoeletric composite depends on the micro-geometry of the phases since one has to provide effective strain coupling and avoid electromagnetic shielding. This has motivated a number of micromechanical models to predict the effective moduli of multiferroic composites. For example, Nan (1994) and Huang and Kuo (1997) used the Green's function method to study a fibrous composite consisting of $BaTiO_3$ and $CoFe_2O_4$. For such transversely isotropic fibrous composites, Benveniste (1995) derived exact connections among effective magnetoelectroelastic moduli based on a formalism discovered by Milgrom and Shtrikman (1989). Particulate composites were investigated by Harshé et al. (1993) using a cubic model and by Lee et al. (2005) using finite element method. Eshelby's approach and the mean field Mori–Tanaka model have been generalized to multiferroic composites by Li and Dunn (1998a,b), Huang (1998), Li (2000), Wu and Huang (2000), Huang and Zhou (2004) and Srinivas et al. (2006). Frequency dependence of magnetoelectric coefficients of multiferroic laminates was studied by Bichurin et al. (2003, 2005). Nan et al. (2008) provide an extensive review of the literature and the state of the art.

However, much of this work uses approximate methods and models based on single inclusions, and focus on the effective properties of composites with somewhat uncontrolled microstructure. There is a need for exact methods that can be used to evaluate these approximate methods. Further, a method that provides the detailed fields is useful

* Corresponding author.
E-mail address: bhatta@caltech.edu (K. Bhattacharya).

0167-6636/$ - see front matter © 2012 Elsevier Ltd. All rights reserved.
http://dx.doi.org/10.1016/j.mechmat.2012.12.004

to provide insights for developing better microstructures and more complex processes like dielectric breakdown and failure (Li and Duxbury, 1989). Similarly, detailed statistical methods require the fields associated with multiple particles (Fassi-Fehri et al., 1989). Furthermore, recent advances in synthesis allows the fabrication of composites with highly controlled microstructure. For example, Ren et al. (2008) have recently used a diblock copolymer precursors to produce a self-assembled hexagonal array of CFO nanofibers in a PZT matrix. Therefore, there is a need for obtaining the fields and properties of composites with controlled microstructure. All of these motivate the current work.

In a classic work, Lord Rayleigh (1892) computed the electric potential for a conducting composite consisting of a periodic array of inclusions (cylinders and spheres). This was extended to arbitrary arrangements by Kuo and Chen (2007, 2008). These works concern single fields. In this paper, we generalize this methodology to multiple coupled fields, specifically electrostatic, magnetostatic and mechanical.

We consider a composite medium made of piezoelectric and piezomagnetic phases arranged in a microstructure consisting of parallel cylinders in a matrix in Section 2. We follow the work of Chen (1993) (also Benveniste, 1995; Zheng and Chen, 1999 Camacho-Montes et al., 2009) and observe in Section 2.1 that if the phases are transversely isotropic, then the general problem can be decomposed into two independent problems, plane strain with transverse electromagnetic fields and anti-plane shear with in-plane electromagnetic fields. We then focus on the latter problem for much of paper. We notice in Section 2.2 that the coupling between the fields occurs only through the interface conditions. We exploit this in Section 2.3 to obtain a representation of the solution. The basic idea is to follow Kuo and Chen (2008) and expand each field in each medium in a series.

While we have developed a direct strategy to solve the coupled problem, we note that there is an alternate strategy. Milgrom and Shtrikman (1989) (also, Benveniste, 1997; Chen, 1997; Milgrom, 1997; Milton., 2001) show that it is possible to transform the coupled problem to the uncoupled problem for a two-phase composite. The transformed problem could then be solved by the approach of Kuo and Chen (2007, 2008). However, this transform approach can *not* be generalized to N-phase composites for $N > 2$. Furthermore the solution is in the transformed domain, and therefore it is difficult to develop insights into the field. The direct approach we develop here overcomes these difficulties.

We specialize to periodic arrays in Section 3. We obtain effective properties in Section 4, and significantly show that the macroscopic properties depend solely on a single expansion coefficient (amongst the infinite).

This methodology is illustrated in Section 5 using composites of $BaTiO_3$ (BTO) and $CoFe_2O_4$ (CFO). We choose this material pair for its practical potential and also because it enables comparison with previous work. We observe that the composite medium has a nontrivial magnetoelectric coupling even though the individual components do not. Further, we observe significant difference between composites with BTO fibers in a CFO matrix and its complement.

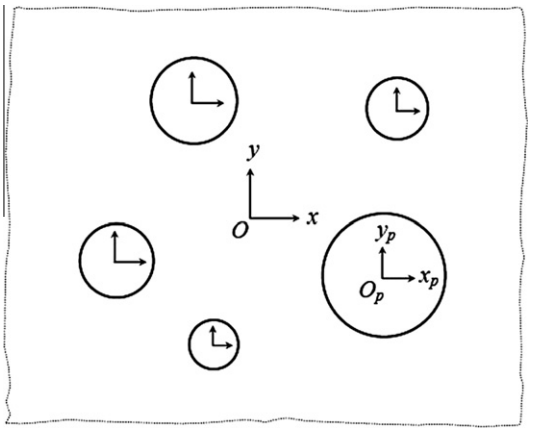

Fig. 1. The cross-section of the fiber composite.

We briefly comment on the first problem – the plane elasticity with transverse electromagnetic fields – in Section 6 and show the opportunity for extremely large magnetoelectric coupling.

2. Arbitrary arrangement of circular cylinders

2.1. General setting

Let us consider an infinite medium $\mathbb{R}^3$containing N arbitrarily distributed, parallel and separated circular cylinders (Fig. 1). The domain of the pth circular cylinder is denoted $V_p, p = 1, 2, \ldots, N$, and the remaining matrix is denoted Ω_m. We assume that the cylinders and the matrix are made of distinct phases.[1] Further, we assume that each phase is either piezoelectric or piezomagnetic. The constitutive laws for the rth phase is given by (see Alshits et al., 1992, for example)

$$\begin{aligned}\boldsymbol{\sigma}^{(r)} &= \mathbf{C}^{(r)}\boldsymbol{\varepsilon}^{(r)} - \mathbf{e}^{T(r)}\mathbf{E}^{(r)} - \mathbf{q}^{T(r)}\mathbf{H}^{(r)},\\ \mathbf{D}^{(r)} &= \mathbf{e}^{(r)}\boldsymbol{\varepsilon}^{(r)} + \boldsymbol{\kappa}^{(r)}\mathbf{E}^{(r)} + \boldsymbol{\lambda}^{T(r)}\mathbf{H}^{(r)},\\ \mathbf{B}^{(r)} &= \mathbf{q}^{(r)}\boldsymbol{\varepsilon}^{(r)} + \boldsymbol{\lambda}^{(r)}\mathbf{E}^{(r)} + \boldsymbol{\mu}^{(r)}\mathbf{H}^{(r)},\end{aligned} \tag{1}$$

where $\boldsymbol{\sigma}$, $\mathbf{D}$, $\mathbf{B}$, $\boldsymbol{\varepsilon}$, $\mathbf{E}$ and $\mathbf{H}$ are the stress, electric displacement, magnetic flux, strain, electric field, and the magnetic field respectively. $\mathbf{C}$ is the fourth-order tensor of elastic moduli, and $\boldsymbol{\kappa}$, $\boldsymbol{\mu}$ and $\boldsymbol{\lambda}$ are the second order tensors of dielectric permittivity, magnetic permeability and magnetoelectric coefficients. $\mathbf{e}$ and $\mathbf{q}$ are piezoelectric and piezomagnetic constants.

Now assume that each phase is transversely isotropic (i.e., has 6 mm symmetry) with the symmetry axes oriented with the cylinders. We introduce a Cartesian coordinate system with the x- and y-axes in the plane of the cross-section and z-along the axes of the cylinders. In the Voigt notation the properties $\mathbf{C}$, $\mathbf{e}$, $\mathbf{q}$, $\boldsymbol{\kappa}$, $\boldsymbol{\mu}$, and $\boldsymbol{\lambda}$ are given by Nye (1985):

[1] Later we shall specialize to a two-phase situation where all the cylinders belong to one phase and the matrix to another.

$$\mathbf{C}^{(r)} = \begin{pmatrix} C_{11} & C_{12} & C_{13} & 0 & 0 & 0 \\ C_{12} & C_{11} & C_{13} & 0 & 0 & 0 \\ C_{13} & C_{13} & C_{33} & 0 & 0 & 0 \\ 0 & 0 & 0 & C_{44} & 0 & 0 \\ 0 & 0 & 0 & 0 & C_{44} & 0 \\ 0 & 0 & 0 & 0 & 0 & C_{66} \end{pmatrix}^{(r)},$$
$$\mathbf{e}^{(r)} = \begin{pmatrix} 0 & 0 & 0 & 0 & e_{15} & 0 \\ 0 & 0 & 0 & e_{15} & 0 & 0 \\ e_{31} & e_{31} & e_{33} & 0 & 0 & 0 \end{pmatrix}^{(r)},$$
$$\mathbf{q}^{(r)} = \begin{pmatrix} 0 & 0 & 0 & 0 & q_{15} & 0 \\ 0 & 0 & 0 & q_{15} & 0 & 0 \\ q_{31} & q_{31} & q_{33} & 0 & 0 & 0 \end{pmatrix}^{(r)},$$
$$\boldsymbol{\kappa}^{(r)} = \begin{pmatrix} \kappa_{11} & 0 & 0 \\ 0 & \kappa_{11} & 0 \\ 0 & 0 & \kappa_{33} \end{pmatrix}^{(r)}, \quad \boldsymbol{\mu}^{(r)} = \begin{pmatrix} \mu_{11} & 0 & 0 \\ 0 & \mu_{11} & 0 \\ 0 & 0 & \mu_{33} \end{pmatrix}^{(r)}, \quad \boldsymbol{\lambda}^{(r)} = \begin{pmatrix} \lambda_{11} & 0 & 0 \\ 0 & \lambda_{11} & 0 \\ 0 & 0 & \lambda_{33} \end{pmatrix}^{(r)}. \tag{2}$$

Consistent with known material properties, the magnetoelectric coupling coefficients $\boldsymbol{\lambda}^{(r)}$ is negligible though we do not explicitly use this fact here.

To obtain the effective properties of this medium, we need to solve for equilibrium equations

$$\nabla \cdot \boldsymbol{\sigma} = \mathbf{0}, \quad \nabla \cdot \mathbf{D} = 0, \quad \nabla \cdot \mathbf{B} = 0, \tag{3}$$

along with the analogous interfacial conditions and appropriate boundary conditions.

We follow Chen (1993) (also Benveniste, 1995; Zheng and Chen, 1999; Camacho-Montes et al., 2009) and show in the appendix that for this cylindrical geometry and transversely isotropic material symmetry, the problem splits naturally into two *independent* problems:

- Plane strain and transverse electromagnetic fields

$$\mathbf{u} = \begin{pmatrix} u_x(x,y) \\ u_y(x,y) \\ 0 \end{pmatrix}, \quad \mathbf{E} = \begin{pmatrix} 0 \\ 0 \\ E_z(x,y) \end{pmatrix}, \quad \mathbf{H} = \begin{pmatrix} 0 \\ 0 \\ H_z(x,y) \end{pmatrix}, \tag{4}$$

- Anti-plane shear and in-plane electromagnetic fields

$$\mathbf{u} = \begin{pmatrix} 0 \\ 0 \\ u_z(x,y) \end{pmatrix}, \quad \mathbf{E} = \begin{pmatrix} E_x(x,y) \\ E_y(x,y) \\ 0 \end{pmatrix}, \quad \mathbf{H} = \begin{pmatrix} H_x(x,y) \\ H_y(x,y) \\ 0 \end{pmatrix}. \tag{5}$$

Therefore, it is sufficient to treat each of these problems. In this work, we largely focus on the second, i.e., anti-plane shear with in-plane electromagnetic fields with brief comments on the first in Section 6.

2.2. Anti-plane shear with in-plane electromagnetic fields

We consider

$$\begin{aligned} &u_x = u_y = 0, u_z = w(x,y), \\ &\varphi = \varphi(x,y), \\ &\psi = \psi(x,y), \end{aligned} \tag{6}$$

where u_x, u_y, u_z are the mechanical displacements along the x-, y-, and z-axes, and φ and ψ are the electric and magnetic potentials, respectively. The constitutive laws of the constituents and of the composite for the non-vanishing fields can be recast in the form

$$\begin{pmatrix} \sigma_{zj} \\ D_j \\ B_j \end{pmatrix} = \begin{pmatrix} C_{44} & e_{15} & q_{15} \\ e_{15} & -\kappa_{11} & -\lambda_{11} \\ q_{15} & -\lambda_{11} & -\mu_{11} \end{pmatrix} \begin{pmatrix} \varepsilon_{zj} \\ -E_j \\ -H_j \end{pmatrix} \tag{7}$$

where j denotes the component x, y. We can write this compactly as

$$\boldsymbol{\Sigma}^j_{\Phi} = L_{\Phi\Psi} Z^j_{\Psi}, \quad \Phi, \Psi = w, \varphi, \psi, j = x,\ y, \tag{8}$$

where

$$\boldsymbol{\Sigma}^j = \begin{pmatrix} \sigma_{zj} \\ D_j \\ B_j \end{pmatrix}, \mathbf{L} = \begin{pmatrix} C_{44} & e_{15} & q_{15} \\ e_{15} & -\kappa_{11} & -\lambda_{11} \\ q_{15} & -\lambda_{11} & -\mu_{11} \end{pmatrix}, \mathbf{Z}^j = \begin{pmatrix} \varepsilon_{zj} \\ -E_j \\ -H_j \end{pmatrix}. \tag{9}$$

The shear strains ε_{zx} and ε_{zy}, in-plane electric fields E_x and E_y, and in-plane magnetic fields H_x and H_y can be derived from the gradient of elastic displacement, electric potential, and magnetic potential as follows:

$$\begin{aligned} &\varepsilon_{zx} = \frac{\partial w}{\partial x}, \varepsilon_{zy} = \frac{\partial w}{\partial y}, \\ &E_x = -\frac{\partial \varphi}{\partial x}, E_y = -\frac{\partial \varphi}{\partial y}, \\ &H_x = -\frac{\partial \psi}{\partial x}, H_y = -\frac{\partial \psi}{\partial y}. \end{aligned} \tag{10}$$

In the absence of body force, electric charge density and electric current density, the equilibrium equations are given by

$$\begin{aligned} &\frac{\partial \sigma_{zx}}{\partial x} + \frac{\partial \sigma_{zy}}{\partial y} = 0, \\ &\frac{\partial D_x}{\partial x} + \frac{\partial D_y}{\partial y} = 0, \\ &\frac{\partial B_x}{\partial x} + \frac{\partial B_y}{\partial y} = 0. \end{aligned} \tag{11}$$

Substitution of Eq. (8) into Eq. (11) yields,

$$\begin{aligned} &C_{44}\nabla^2 w + e_{15}\nabla^2 \varphi + q_{15}\nabla^2 \psi = 0, \\ &e_{15}\nabla^2 w - \kappa_{11}\nabla^2 \varphi - \lambda_{11}\nabla^2 \psi = 0, \\ &q_{15}\nabla^2 w - \lambda_{11}\nabla^2 \varphi - \mu_{11}\nabla^2 \psi = 0, \end{aligned} \tag{12}$$

where $\nabla^2 = \partial^2/\partial x^2 + \partial^2/\partial y^2$ represents the two-dimensional Laplace operator for the variable x and y. Since $\mathbf{L}$ is a nonsingular matrix, generically we can decouple (12) into three independent Laplace equations,

$$\nabla^2 w = 0, \quad \nabla^2 \varphi = 0, \quad \text{and} \quad \nabla^2 \psi = 0 \tag{13}$$

in the interior of each phase. In other words, the three fields – displacement, electrostatic potential and magnetostatic potential – are completely decoupled in the interior of each phase.

In addition to these differential equations, we have to use interface and boundary conditions. We assume that the interfaces are perfectly bonded, and therefore the fields satisfy

$$[[\boldsymbol{\Sigma}^j \mathbf{n}^j]] = [[(\mathbf{L}\mathbf{Z}^j)\mathbf{n}^j]] = 0, \qquad [[\mathbf{Z}^j \mathbf{t}^j]] = 0 \tag{14}$$

where $[[\cdot]]$ denotes the jump in some quantity across the interface, $\mathbf{n}$ is the unit normal to the interface and $\mathbf{t}$ is

the unit tangent to the interface, and the repeated index j denotes summing over the components x, y. Since $\mathbf{L}$ is different in the two phases, the fields w, φ and ψ are generally coupled by the interface equations.

2.3. Representation of the solution

In the anti-plane shear problem, we showed above that the fields are decoupled in the interior of every phase, but are coupled at the interfaces. Therefore, we may follow Kuo and Chen (2008) and use a series expansion for each field in the interior of each phases and then obtain the coefficients by enforcing the interface and boundary conditions.

We consider a situation where the composite is subjected to a macroscopically uniaxial loading

$$w_{\text{ext}} = \overline{\varepsilon}_{zx} x, \quad \varphi_{\text{ext}} = -\overline{E}_x x, \quad \psi_{\text{ext}} = -\overline{H}_x x, \tag{15}$$

for constants $\overline{\varepsilon}_{zx}$, $\overline{E}_x$ and $\overline{H}_x$. We may rewrite this in short as

$$\Phi_{\text{ext}} = \overline{Z}^x_\Phi x, \tag{16}$$

where Φ represents the appropriate field – the anti-plane deformation w, electric potential φ, or magnetic potential ψ– and $\overline{Z}^x_\Phi$ the corresponding applied field – $\overline{\varepsilon}_{zx}, -\overline{E}_x$, or $-\overline{H}_x$.

We rewrite the governing equation, Eq. (13) in polar coordinates (r, θ),

$$\nabla^2 \Phi = \frac{\partial^2 \Phi}{\partial r^2} + \frac{1}{r}\frac{\partial \Phi}{\partial r} + \frac{1}{r^2}\frac{\partial^2 \Phi}{\partial \theta^2} = 0, \tag{17}$$

where Φ can be w, φ or ψ. The potential field for the pth circular cylinder and its surrounding matrix can be expanded with respect to its center O_p as

$$\Phi_i^{(p)} = C_0^{\Phi(p)} + \sum_{n=1}^{\infty}\left(C_n^{\Phi(p)} r_p^n \cos n\theta_p + F_n^{\Phi(p)} r_p^n \sin n\theta_p\right) \tag{18}$$

for the inclusion, and

$$\Phi_m^{(p)} = A_0^{\Phi(p)} + \sum_{n=1}^{\infty}\left[\left(A_n^{\Phi(p)} r_p^n + B_n^{\Phi(p)} r_p^{-n}\right)\cos n\theta_p + \left(D_n^{\Phi(p)} r_p^n + E_n^{\Phi(p)} r_p^{-n}\right)\sin n\theta_p\right] \tag{19}$$

for the matrix. Here (r_p, θ_p) is the local polar coordinate centered at the origin of the pth circle, the subscripts i and m denote the inclusion and matrix, respectively. The coefficients $A_n^{\Phi(p)}, B_n^{\Phi(p)}, \ldots, F_n^{\Phi(p)}$ are some unknowns to be determined. The superscripts p in (18) and (19) indicate that the fields that are expanded with respect to the pth cylinder center.

We recall the interface conditions (14) which we rewrite as

$$\Phi_m^{(p)}\Big|_{\partial V_p} = \Phi_i^{(p)}\Big|_{\partial V_p}, \quad (\boldsymbol{\Sigma}_\Phi)_m^{(p)} \cdot \mathbf{n}_p\Big|_{\partial V_p} = (\boldsymbol{\Sigma}_\Phi)_i^{(p)} \cdot \mathbf{n}_p\Big|_{\partial V_p} \tag{20}$$

where

$$\boldsymbol{\Sigma}_w = (\sigma_{zx}, \sigma_{zy}), \boldsymbol{\Sigma}_\varphi = (D_x, D_y), \boldsymbol{\Sigma}_\psi = (B_x, B_y), \tag{21}$$

$\partial V_p : r_p = a_p$ denotes the interface between the matrix and the pth circular cylinder, and $\mathbf{n}_p$ is the unit outward normal of the interface ∂V_p.

Using the orthogonality properties of trigonometric functions, the conditions (20) provide

$$\mathbf{a}_n^{(p)} = a_p^{-2n}\mathbf{T}^{(p)}\mathbf{b}_n^{(p)}, \mathbf{c}_n^{(p)} = a_p^{-2n}\left(\mathbf{T}^{(p)} + \mathbf{I}\right)\mathbf{b}_n^{(p)}, \tag{22}$$

$$\mathbf{d}_n^{(p)} = a_p^{-2n}\mathbf{T}^{(p)}\mathbf{e}_n^{(p)}, \mathbf{f}_n^{(p)} = a_p^{-2n}\left(\mathbf{T}^{(p)} + \mathbf{I}\right)\mathbf{e}_n^{(p)}, \tag{23}$$

and $A_0^{\Phi(p)} = C_0^{\Phi(p)}$, where

$$\mathbf{a}_n^{(p)} = \begin{pmatrix} A_n^{w(p)} \\ A_n^{\varphi(p)} \\ A_n^{\psi(p)} \end{pmatrix}, \mathbf{b}_n^{(p)} = \begin{pmatrix} B_n^{w(p)} \\ B_n^{\varphi(p)} \\ B_n^{\psi(p)} \end{pmatrix}, \mathbf{c}_n^{(p)} = \begin{pmatrix} C_n^{w(p)} \\ C_n^{\varphi(p)} \\ C_n^{\psi(p)} \end{pmatrix}, \tag{24}$$

$$\mathbf{d}_n^{(p)} = \begin{pmatrix} D_n^{w(p)} \\ D_n^{\varphi(p)} \\ D_n^{\psi(p)} \end{pmatrix}, \mathbf{e}_n^{(p)} = \begin{pmatrix} E_n^{w(p)} \\ E_n^{\varphi(p)} \\ E_n^{\psi(p)} \end{pmatrix}, \mathbf{f}_n^{(p)} = \begin{pmatrix} F_n^{w(p)} \\ F_n^{\varphi(p)} \\ F_n^{\psi(p)} \end{pmatrix}, \tag{25}$$

$$\mathbf{T}^{(p)} = \left(\mathbf{L}^{(m)} - \mathbf{L}^{(p)}\right)^{-1}\left(\mathbf{L}^{(m)} + \mathbf{L}^{(p)}\right), \tag{26}$$

and $\mathbf{I}$ is the 3×3 identity tensor.

We now need to relate the solutions to the applied boundary conditions. We do so by applying the Green's second identity (Arfken and Weber, 2001) to the matrix domain Ω_m. This gives

$$\int_{\Omega_m}\left[G(\mathbf{x};\mathbf{x}')\nabla'^2\Phi_m(\mathbf{x}') - \Phi_m(\mathbf{x}')\nabla'^2 G(\mathbf{x};\mathbf{x}')\right]dA' = \int_{\partial\Omega_m}\left[G(\mathbf{x};\mathbf{x}')\nabla'\Phi_m(\mathbf{x}') - \Phi_m(\mathbf{x}')\nabla' G(\mathbf{x};\mathbf{x}')\right]\cdot\mathbf{n}'ds', \tag{27}$$

where the prime $'$ denotes the operation in reference to the $\mathbf{x}'$ coordinate, $\mathbf{n}'$ is the outward unit normal to the matrix's boundary $\partial\Omega_m$, dA' represents the area element for the $\mathbf{x}'$ coordinate, ds' is the differential arc length. Here $G(\mathbf{x};\mathbf{x}')$ is the free-space Green's function for Laplace operator satisfying $\nabla^2 G(\mathbf{x};\mathbf{x}') = -\delta(\mathbf{x}-\mathbf{x}')$, where $\delta(\mathbf{x}-\mathbf{x}')$ is the Dirac-delta distribution. Following the procedure in Kuo and Chen (2008), it can be shown that Eq. (27) yields

$$\Phi_m(\mathbf{x}) = \Phi_{\text{ext}}(\mathbf{x}) + \sum_{l=1}^{N}\sum_{m=1}^{\infty}\left(B_m^{\Phi(l)} r_l^{-m}\cos m\theta_l + E_m^{\Phi(l)} r_l^{-m}\sin m\theta_l\right). \tag{28}$$

This is the consistency equation which relates the external applied fields to the local potential expansions.

For convenience, we introduce the complex variable notation $z = x + iy$ for $\mathbf{x} = (x, y)$ with respect to the matrix and z_p for the cylinder centered at O_p. Now, Eq. (28) can be rewritten as

$$\Phi_m(\mathbf{x}) = \overline{Z}^x_\Phi z + \sum_{l=1}^{N}\sum_{m=1}^{\infty}\left[B_m^{\Phi(l)}\text{Re}(z-z_l)^{-m} - E_m^{\Phi(l)}\text{Im}(z-z_l)^{-m}\right], \tag{29}$$

where $\overline{Z}^x_\Phi$ represents the corresponding applied field $\overline{\varepsilon}_{zx}, -\overline{E}_x$, or $-\overline{H}_x$. Note that the field identity (29) is written based on different coordinates. To proceed, we shift the origin of the expansions (29) to a fixed point, say z_p. For point z satisfying the inequality $|z - z_p| < |z_p - z_l|$, we can then expand the term $(z - z_l)^{-m}$ using the binomial theorem as Arfken and Weber (2001)

$$(z-z_l)^{-m}=\sum_{s=0}^{\infty}(-1)^s\binom{m+s-1}{s}\frac{(z-z_p)^s}{(z_p-z_l)^{m+s}}. \tag{30}$$

Introducing (30) into (29), we have the expansion

$$\begin{aligned}\Phi^{(p)}_{m,near}(\mathbf{x})&=\overline{Z}^x_\Phi \mathrm{Re} z_p+\overline{Z}^x_\Phi \mathrm{Re}(z-z_p)\\&+\sum_{m=1}^{\infty}\left[B^{\Phi(p)}_m \mathrm{Re}(z-z_p)^{-m}-E^{\Phi(p)}_m \mathrm{Im}(z-z_p)^{-m}\right]\\&+\sum_{l\neq p}\sum_{s=0}^{\infty}\sum_{m=1}^{\infty}(-1)^s\binom{m+s-1}{s}\\&\times\left[B^{\Phi(l)}_m \mathrm{Re}\frac{(z-z_p)^s}{(z_p-z_l)^{m+s}}-E^{\Phi(l)}_m \mathrm{Im}\frac{(z-z_p)^s}{(z_p-z_l)^{m+s}}\right]\end{aligned} \tag{31}$$

valid for the domain

$$|z-z_p|<\min\left(|z_p-z_l|\right),\ \text{for } l=1,2,\ldots,N, p\neq l. \tag{32}$$

Since the expansion (31) are valid for points satisfying the condition (32), which generally applies to points near the pth inclusion, this expansion will be referred to as a near-field expansion, denoted as $\Phi^{(p)}_{m,near}(\mathbf{x})$. Further, since $\mathbf{x}$ lies in the matrix domain, Eqs. (31) and (19) should be identical. This provides the condition

$$\begin{aligned}&A^{\Phi(p)}_0+\sum_{n=1}^{\infty}\left[A^{\Phi(p)}_n \mathrm{Re}(z-z_p)^n+D^{\Phi(p)}_n \mathrm{Im}(z-z_p)^n\right]\\&=\overline{Z}^x_\Phi \mathrm{Re} z_p+\overline{Z}^x_\Phi \mathrm{Re}(z-z_p)+\sum_{l\neq p}\sum_{s=0}^{\infty}\sum_{m=1}^{\infty}(-1)^s\binom{m+s-1}{s}\\&\times\left[B^{\Phi(l)}_m \mathrm{Re}\frac{(z-z_p)^s}{(z_p-z_l)^{m+s}}-E^{\Phi(l)}_m \mathrm{Im}\frac{(z-z_p)^s}{(z_p-z_l)^{m+s}}\right].\end{aligned} \tag{33}$$

Taking the real part and the imaginary part of (33), we find the two conditions

$$\begin{aligned}&A^{\Phi(p)}_n-\sum_{l\neq p}\sum_{m=1}^{\infty}(-1)^n\binom{m+n-1}{n}\\&\times\left[B^{\Phi(l)}_m \mathrm{Re}(z_p-z_l)^{-m-n}-E^{\Phi(l)}_m \mathrm{Im}(z_p-z_l)^{-m-n}\right]\\&=\overline{Z}^x_\Phi \mathrm{Re} z_p\delta_{n,0}+\overline{Z}^x_\Phi\delta_{n,1},\end{aligned} \tag{34}$$

and

$$\begin{aligned}&D^{\Phi(p)}_n+\sum_{l\neq p}\sum_{m=1}^{\infty}(-1)^n\binom{m+n-1}{n}\\&\times\left[B^{\Phi(l)}_m \mathrm{Im}(z_p-z_l)^{-m-n}+E^{\Phi(l)}_m \mathrm{Re}(z_p-z_l)^{-m-n}\right]=0.\end{aligned} \tag{35}$$

Eqs. (34), (35), $(22)_1$, and $(23)_1$ constitute an infinite set of linear algebraic equations. Upon appropriate truncations of the expansion terms, we can determine the expansion coefficients $A^{\Phi(p)}_n, B^{\Phi(p)}_n, \ldots, F^{\Phi(p)}_n$.

3. Periodic arrays

The analysis carried out in the previous section for the arbitrary system with a finite number of cylinders may also be adapted for the case of a periodic array of cylinders. Relevant works in magnetoelectric composites with periodic configurations include, for example, Aboudi (2001), who developed a homogenization method for the prediction of the effective properties of magneto-electro-thermo-elastic composites and the results are in good agreement with those of the Mori–Tanaka model. Lee et al. (2005) proposed a finite element analysis based micromechanics approach to determine the effective material properties of three-phase electromagnetoelastic composites. A variational asymptotic method has been used by Tang and Yu (2008, 2009) to construct a fully coupled micromechanics model for prediction of effective behaviours and local fields of smart composites. Camacho-Montes et al. (2009) adopted a two-scale asypmtotic homogenization method to determine the overall behaviour of magnetoelectric coupling and cross-property connections in a square array of a binary composite.

There are five possible ways of packing cylinders in regular arrays in two dimensions (see Kittel, 1986, for instance). Here we concentrate on the two lattices, rectangular and hexagonal. It is known that in the case of elasticity, a hexagonal arrangement of circular fibers results in effective transverse isotropy; on the other hand a square arrangement results in general in square symmetry (Li., 2000). It turns out however that in the case of conduction square symmetry and transverse isotropy become identical, and both kinds of arrangements give therefore rise to the same overall symmetry (Perrins et al., 1979). This statement is also correct for piezomagnetoelectricity under anti-plane shear with in-plane electromagnetic fields which is the case of our study. We sketch the outline of the derivation focussing on the differences from the previous situation. Finally, we limit ourselves to the case of anti-plane shear with in-plane electromagnetic fields.

Let us first introduce a Cartesian coordinate system (x,y) positioned at the center O of one of the cylinders in a square or a hexagonal array, as shown in Fig. 2. The radius of the cylinders is a and we may assume unit distance between the centers of neighboring cylinders without loss of generality. Uniform intensities $\overline{E}_x$ and $\overline{H}_x$ are applied along the positive x axis, and an anti-plane shear deformation $\overline{\varepsilon}_{zx}$ is applied out of the xy plane. In terms of polar coordinates, the general solution has the admissible form

$$\Phi_i=C^\Phi_0+\sum_{n=1}^{\infty}C^\Phi_n r^n\cos n\theta \tag{36}$$

for $r<a$, and

$$\Phi_m=A^\Phi_0+\sum_{n=1}^{\infty}\left(A^\Phi_n r^n+B^\Phi_n r^{-n}\right)\cos n\theta \tag{37}$$

for $r>a$. The coefficients A^Φ_n, B^Φ_n, and C^Φ_n are unknown constants to be determined from the interface and boundary conditions. Note that the sine terms that would be present in a general expansion are missing since we impose a uniaxial loading along the $x-$ direction. Further, $\Phi(r,\theta)$ has to be antisymmetric with respect to the $y-$ axis, and thus only terms with an odd number are included. Finally, for a hexagonal lattice, all terms in which n is a multiple of three are disallowed (Perrins et al., 1979).

Analogous to (22), the continuity conditions at the interface will give constraints (22) between the coefficients.

Next, imposing the periodicity conditions analogous to imposing the boundary condition we did to derive (34), leads to a generalized Rayleigh's identity

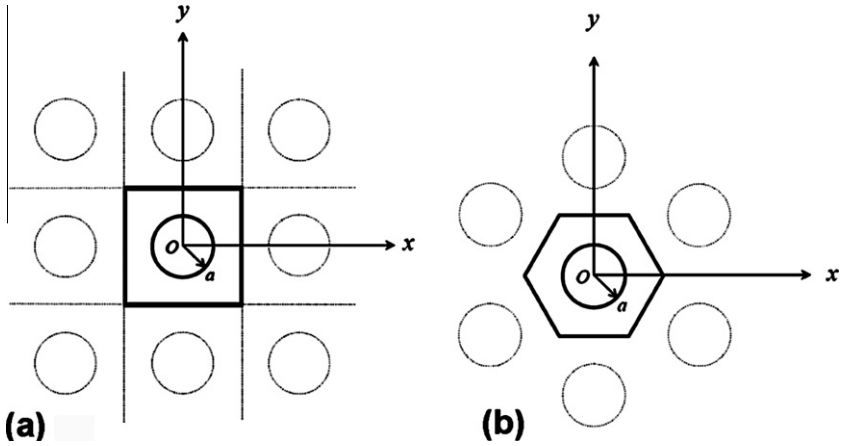

Fig. 2. A schematic representation of a unit cell: (a) a square array, (b) a hexagonal array.

$$A_n^{\Phi} + \sum_{m=1}^{\infty} \binom{m+n-1}{n} S_{m+n} B_m^{\Phi} = \overline{Z}_{\Phi}^{x} \delta_{n,1}. \tag{38}$$

Here the quantities

$$S_m = \sum_{l \neq o} \mathrm{Re} z_l^{-m} \tag{39}$$

are the lattice sums characterizing the geometry of the periodic structure, and z_l is the center of the lth cylinder when measured at the central point O. The index l runs over all cylinders' centers underlying the periodic array except the central one. A list of non-zero normalized lattice sums for square and hexagonal arrays can be found in Berman and Greengard (1994).

Eqs. (38) and $(22)_1$ constitute an infinite set of linear algebraic equations. Upon appropriate truncations of the expansion terms, we can determine the expansion coefficients A_n^{Φ}, B_n^{Φ}, and C_n^{Φ}.

4. Effective moduli

We are interested in the effective behavior for a situation where we have a large number of cylinders. The effective material properties are defined in terms averaged fields,

$$\left\langle \mathbf{\Sigma}^j \right\rangle \equiv \mathbf{L}^* \left\langle \mathbf{Z}^j \right\rangle, \tag{40}$$

where the angular brackets denote the average over the representative volume element (unit cell in the case of periodic composites)

$$\left\langle \mathbf{\Sigma}^j \right\rangle = \frac{1}{V} \int_V \mathbf{\Sigma}^j d\mathbf{x}, \quad \left\langle \mathbf{Z}^j \right\rangle = \frac{1}{V} \int_V \mathbf{Z}^j d\mathbf{x}, \tag{41}$$

and $\mathbf{L}^*$ denotes the effective magnetoelectroelastic parameters of the composite.

We can compute the average $\mathbf{Z}^j$ by noting that each component is a gradient and applying the divergence theorem. We obtain

$$\left\langle Z_{\Phi}^{x} \right\rangle = \overline{Z}_{\Phi}^{x}. \tag{42}$$

Next, to find $\left\langle \Sigma_{\Phi}^{x} \right\rangle$, we again use the divergence theorem and the equilibrium condition (including the interface conditions) to obtain:

$$\begin{aligned} \left\langle \Sigma_{\Phi}^{x} \right\rangle &= \frac{1}{V} \int_V \Sigma_{\Phi}^{x} d\mathbf{x} = \frac{1}{V} \int_V \nabla \cdot (x \mathbf{\Sigma}_{\Phi}) d\mathbf{x} \\ &= \frac{1}{V} \int_{\partial V} x (\mathbf{\Sigma}_{\Phi})_m \cdot \mathbf{n} ds, \end{aligned} \tag{43}$$

where $\mathbf{\Sigma}_{\Phi}$ is defined in (21). We then use the expansions (19) for the fields to obtain

$$\frac{1}{V} \int_{\partial V} x (\mathbf{Z}_{\Phi})_m \cdot \mathbf{n} ds = \overline{Z}_{\Phi}^{x} - 2 \sum_{l=1}^{N} a_l^{-2} f_l B_1^{\Phi(l)}, \tag{44}$$

where

$$\mathbf{Z}_w = (\varepsilon_{zx}, \varepsilon_{zy}), \mathbf{Z}_{\varphi} = -(E_x, E_y), \mathbf{Z}_{\psi} = -(H_x, H_y), \tag{45}$$

and f_l is the volume fraction of phase l defined as $f_l = \pi a_l^2 / V$ for square arrays and is $\frac{2\pi}{\sqrt{3}} a_l^2 / V$ for hexagonal arrays. Putting (43) and (44) together, and recalling the constitutive relation (7) for the matrix, we obtain

$$\begin{pmatrix} \langle \sigma_{zx} \rangle \\ \langle D_x \rangle \\ \langle B_x \rangle \end{pmatrix} = \begin{pmatrix} C_{44} & e_{15} & q_{15} \\ e_{15} & -\kappa_{11} & -\lambda_{11} \\ q_{15} & -\lambda_{11} & -\mu_{11} \end{pmatrix}^{(m)} \begin{pmatrix} \overline{\varepsilon}_{zx} - 2 \sum_{l=1}^{N} a_l^{-2} f_l B_1^{w(l)} \\ -\overline{E}_x - 2 \sum_{l=1}^{N} a_l^{-2} f_l B_1^{\varphi(l)} \\ -\overline{H}_x - 2 \sum_{l=1}^{N} a_l^{-2} f_l B_1^{\psi(l)} \end{pmatrix}. \tag{46}$$

Putting together (40) and (46) and noting that the coefficients B_1^{Φ} depend linearly on the applied field $\overline{Z}_{\Phi}^{x}$, we obtain set of equations for the effective property $\mathbf{L}^*$. We can determine this by applying different loading combinations between $\overline{\varepsilon}_{zx}, \overline{E}_x$ and $\overline{H}_x$.

5. Numerical results and discussion

In order to have a better understanding for the theoretical results above, we perform a numerical computation for a two-phase transversely isotropic piezoelectric-piezomagnetic composite with 6*mm* material symmetry about the fiber axis. Specifically we consider a composite of $BaTiO_3$ and $CoFe_2O_4$ which has been studied by other researchers. We consider square and hexagonal arrays,

Table 1
Material parameters of $BaTiO_3$ and $CoFe_2O_4$ (Li and Dunn, 1998b).

Property	$BaTiO_3$	$CoFe_2O_4$
C_{44} (N/m^2)	43×10^9	45.3×10^9
e_{15} (C/m^2)	11.6	0
q_{15} (N/A m)	0	550
κ_{11} (C^2/N m^2)	11.2×10^{-9}	0.08×10^{-9}
μ_{11} (N s^2/C^2)	5×10^{-6}	-590×10^{-6}
λ_{11} (N s/VC)	0	0

and both cases, i.e., both BTO fibers in a CFO matrix and CFO fibers in a BTO matrix. The independent material constants of these constituents are given in Table 1, where the xy plane is isotropic and the unique axis is along the $z-$direction. Note that in both materials magnetoelectric coefficients are zero, i.e. $\lambda_{11} = 0$.

We begin with a composite of BTO fibers in a CFO matrix. Fig. 3 shows the effective elastic, dielectric, magnetic, piezoelectric, piezomagnetic and magnetoelectric moduli for this composite. They vary nonlinearly with volume fraction, and the curves stop at $f = \pi/4$ and $f = \pi/2\sqrt{3}$ for the square and hexagonal arrays respectively, when the inclusions touch. The magnetoelectric coefficient is non-zero for every (non-zero) volume fraction even though this coefficient is zero for each component. This reflects the coupling of the various fields across the boundary. Further, it initially increases with increasing volume fraction, then reaches a maximum before dropping just as the fibers are close to touching. To gain insight into this behavior, we plot the the contours of displacement, electric potential and magnetic potential for a square array in Fig. 5(a)–(c) with an applied magnetic field. The magnetic field induces a mechanical stress in the CFO which in turn results in an electric displacement in the BTO fiber. The effective electric displacement in the horizontal direction depends on the average along the vertical direction. Thus, the effective electric displacement depends on the span of the fiber in the vertical direction. This is why the ME coefficient starts at zero and increases with volume fraction. The magnetic field is attracted by the BTO (since it has a smaller magnetic permeability) and thus the scaling deviates from being proportional to the span and is close to linear initially. Further, as the particles come close to touching, there is very little CFO to induce stress and thus the ME coefficient drops dramatically.

Finally, Fig. 3 also compares the effective moduli with those predicted by Benveniste (1995) who used the composite cylinder assemblage (CCA) model. In CCA, there is no upper limit on the volume fraction since one can have fibers with various sizes. Still, the overall magnitudes and trends agree well between our periodic and his CCA. Furthermore, the results of our analysis fulfil the compatibility conditions given in Eq. (21) of Benveniste (1995).

We now turn to the composite of CFO fibers in a BTO matrix. Fig. 4 shows the effective moduli for this composite. Again, magnetoelectric coefficient is non-zero for every (non-zero) volume fraction even though this coefficient is zero for each component. However, in this case it is monotone increasing with a sharp rise as the particles are close to touching. Further, we verify our results with the compatibility relation (21) proposed in Benveniste (1995). Again, they are in good agreement. Fig. 5(d)–(f) show the potential contours for an applied magnetic field. Now, the magnetic field is expelled by the fibers giving rise to a displacement which deforms the matrix to induce an electric displacement. The amount of deformation it can cause in the matrix increases with volume fraction, and this is reflected in the magnetoelectric coeffecient. Further, it increases dramatically as the particles touch.

We finally turn to the magnetoelectric voltage coefficient, which is the important figure of merit for magnetic field sensors. It relates the overall electric field that is generated in the composite when it is subjected to a magnetic field. It combines the coupling and dielectric coefficients, and is defined by

$$\alpha^*_{E11} = \lambda^*_{11}/\kappa^*_{11}. \tag{47}$$

Fig. 6 shows how this coefficient depends on the volume fraction for the various cases. Note that there is a qualitative difference between the case of BTO fibers in CFO and its complement. In the former, the maximum coefficient is for an intermediate volume fraction of $f = 0.35$ where $\alpha^*_{E11} = 0.0306$ V/cm Oe independent of the square or hexagonal geometry. In contrast, in the case of CFO fibers in the BTO matrix, the maximum is attained as the fibers begin to touch. These trends are similar to those of the magnetoelectric coefficient described before, and follow from the same reasons.

6. Plane strain with transverse electromagnetic fields

We briefly discuss the other problem described in (4), and the potential for using it for large effective magnetoelectric coefficient. Consider a situation where the average normal stress as well as the average electric displacement along the fibers are zero

$$\langle \sigma_{zz} \rangle = 0, \quad \langle D_z \rangle = 0. \tag{48}$$

The constitutive Eqs. (2) specialized to the current setting (see (A.1) and (A.2)) then implies that

$$\langle C_{33} \rangle \varepsilon_{zz} = -\langle C_{13}(\varepsilon_{xx} + \varepsilon_{yy}) \rangle + \langle e_{33} \rangle E_z + \langle q_{33} \rangle H_z, \tag{49}$$

$$\langle e_{33} \rangle \varepsilon_{zz} = -\langle e_{31}(\varepsilon_{xx} + \varepsilon_{yy}) \rangle - \langle \kappa_{33} \rangle E_z - \langle \lambda_{33} \rangle H_z. \tag{50}$$

Eliminating ε_{zz} between the two equations above, we obtain

$$\frac{\langle e_{33} \rangle}{\langle C_{33} \rangle}\left(-\langle C_{13}(\varepsilon_{xx} + \varepsilon_{yy}) \rangle + \langle e_{33} \rangle E_z + \langle q_{33} \rangle H_z\right) = -\langle e_{31}(\varepsilon_{xx} + \varepsilon_{yy}) \rangle - \langle \kappa_{33} \rangle E_z - \langle \lambda_{33} \rangle H_z, \tag{51}$$

or

$$\left(\frac{\langle e_{33} \rangle^2}{\langle C_{33} \rangle} + \langle \kappa_{33} \rangle\right) E_z = \frac{\langle e_{33} \rangle \langle C_{13}(\varepsilon_{xx} + \varepsilon_{yy}) \rangle}{\langle C_{33} \rangle} - \langle e_{31}(\varepsilon_{xx} + \varepsilon_{yy}) \rangle - \left(\frac{\langle e_{33} \rangle \langle q_{33} \rangle}{\langle C_{33} \rangle} + \langle \lambda_{33} \rangle\right) H_z. \tag{52}$$

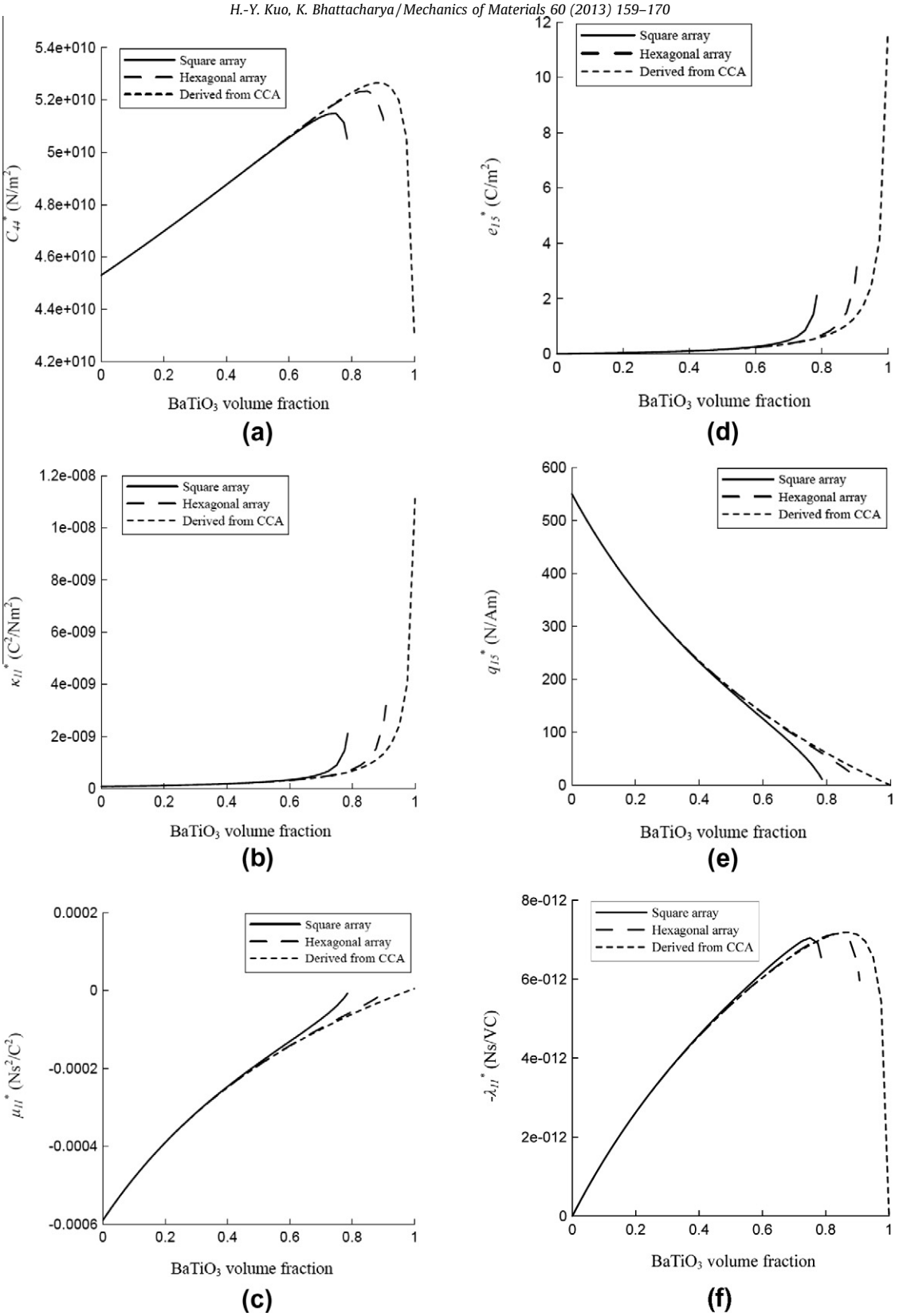

Fig. 3. Effective moduli of a composite of BTO fibers in a CFO matrix versus BTO fiber volume fractions: (a) effective elastic modulus, (b) effective dielectric permittivity, (c) effective magnetic permeability, (d) effective piezoelectric modulus, (e) effective piezomagnetic modulus, and (f) effective magnetoelectric coefficient.

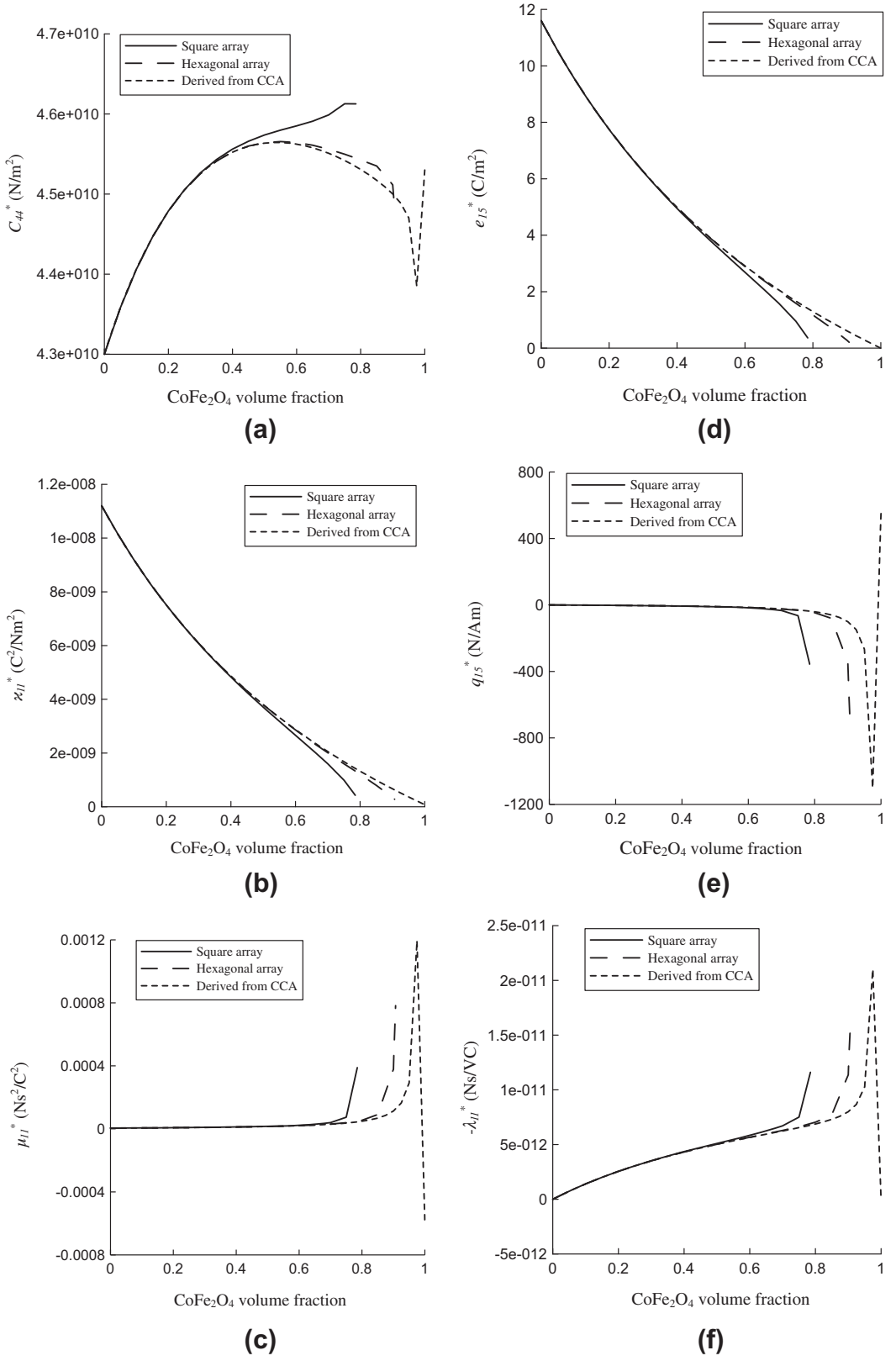

Fig. 4. Effective moduli of a composite of CFO fibers in a BTO matrix versus CFO fiber volume fractions: (a) effective elastic modulus, (b) effective dielectric permittivity, (c) effective magnetic permeability, (d) effective piezoelectric modulus, (e) effective piezomagnetic modulus, (f) effective magnetoelectric coefficient.

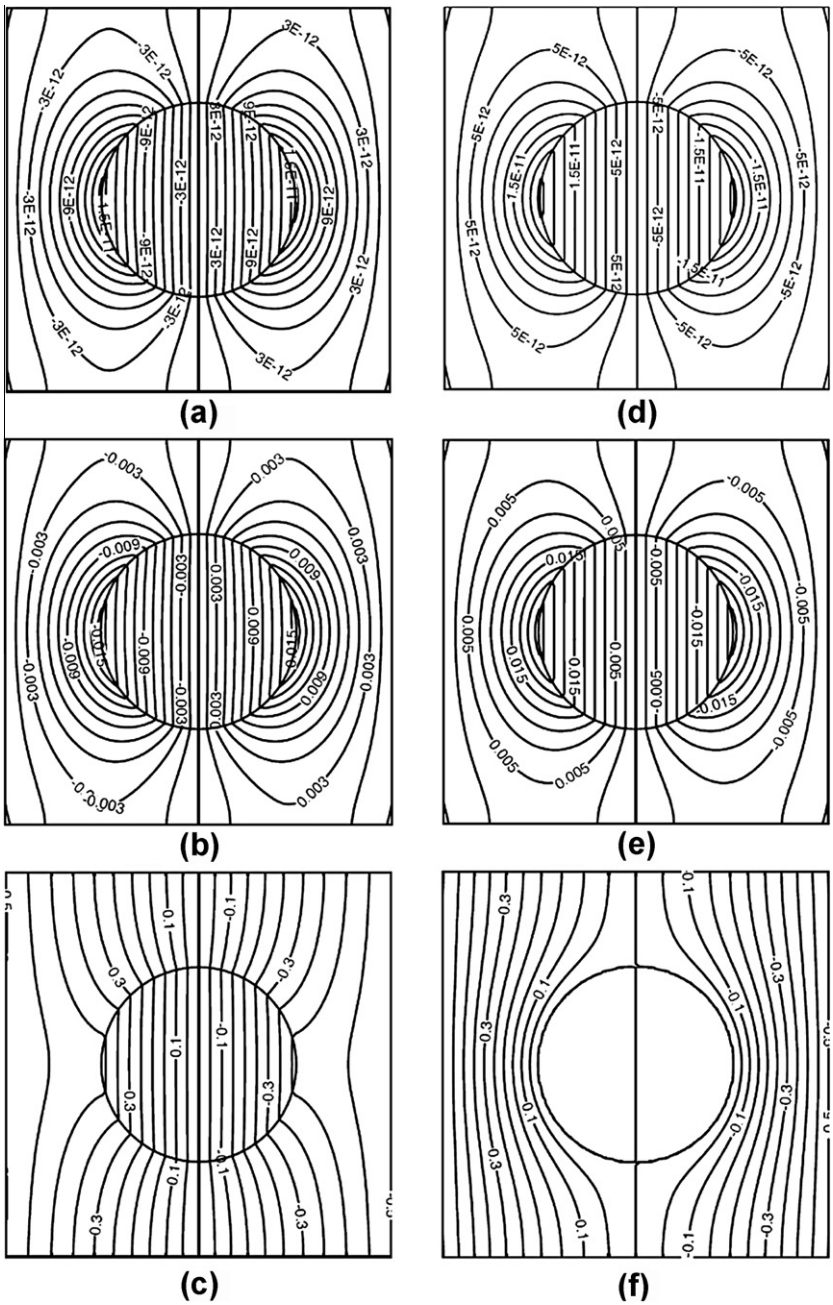

Fig. 5. Potential contours for a square array composite ($f = 0.2$, $\overline{\varepsilon}_{zx} = 0$, $\overline{E}_x = 0$, $\overline{H}_x = 1C/ms$) (a–c) BTO fibers embedded in a CFO matrix, (d–f) CFO fibers embedded in a BTO matrix, (a, d) Vertical displacement (m), (b, e) Electric potential (V), (c, f) Magnetic potential (C/s).

We now assume further that the average planar strain is zero (alternately, we can proceed exactly the same if the effective planar stress is zero). Then, strain depends linearly on E_z and H_z, and thus, we can write

$$\frac{\langle e_{33}\rangle\langle C_{13}(\varepsilon_{xx}+\varepsilon_{yy})\rangle}{\langle C_{33}\rangle} - \langle e_{31}(\varepsilon_{xx}+\varepsilon_{yy})\rangle = AE_z + BH_z. \tag{53}$$

A and B depend on the solution of the plane strain homogenization problem. Substituting (53) into (52), we obtain

$$\left(\frac{\langle e_{33}\rangle^2}{\langle C_{33}\rangle} - A + \langle \kappa_{33}\rangle\right)E_z = \left(B - \frac{\langle e_{33}\rangle\langle q_{33}\rangle}{\langle C_{33}\rangle} - \langle \lambda_{33}\rangle\right)H_z. \tag{54}$$

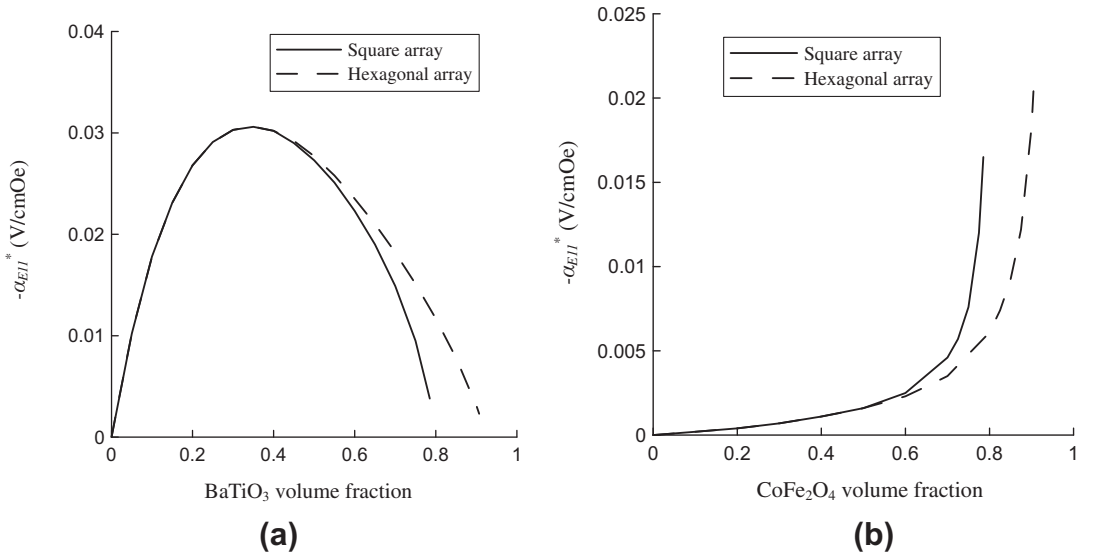

Fig. 6. Effective magnetoelectric voltage coefficient of the composite versus the fiber volume fraction: (a) BTO fibers in a CFO matrix, (b) CFO fibers in a BTO matrix.

The magnetoelectric voltage coefficient is the ratio of the two terms in parenthesis,

$$\alpha^*_{E33} = \frac{B - \frac{\langle e_{33}\rangle\langle q_{33}\rangle}{\langle C_{33}\rangle} - \langle \lambda_{33}\rangle}{\frac{\langle e_{33}\rangle^2}{\langle C_{33}\rangle} - A + \langle \kappa_{33}\rangle}. \tag{55}$$

In particular, we concentrate on the denominator. Notice that only A depends on the microgeometry and the planar moduli where as the rest of the terms do not. Thus, it is possible to tune the microgeometry to reduce the denominator to get extremely large coupling.

We may use the methodology described in this paper to compute A and B. However, in contrast to anti-plane shear, plane strain elasticity is a vectorial problem and thus the method is significantly more difficult to implement. This is the topic of current work and will be presented elsewhere.

7. Concluding remarks

In summary, we have extended Rayleigh's formulation on periodic conductive composites to a magnetoelectroelastic composite consisting of arbitrarily distributed or periodic arrays of cylinders under anti-plane shear deformation, in-plane electric and in-plane magnetic intensities. Expressions for the elastic, electric and magnetic potentials for the cylinders and the matrix are derived, and used to compute the effective moduli. It is shown that the effective properties solely depend on one particular constant B_1^{Φ} among the infinite number of expansion coefficients. Finally, as a practical example, explicit numerical calculations for field distributions and the magnetoelectric effects in $BaTiO_3$–$CoFe_2O_4$ composites are presented and discussed. This example shows the important difference between the case of BTO fibers in a CFO matrix from its complement. The present theoretical framework provides a general guideline for the selection of the best combination with an efficient coupling of piezoelectric and piezomagnetic properties. It can also provide a rigorous basis against which several approximate micromechanical models can be compared.

Acknowledgment

This work was conducted while H.-Y. Kuo held a visit at the California Institute of Technology. We are grateful to National Science Council, Taiwan, under contract NSC-0-95-SAF-I-564-622-TMS for the Taiwan Merit Scholarship that enabled this visit. We are also grateful to the financial support of the US Army Research Office (W911NF-07–1-0410).

Appendix A

We substitute Eq. (2) into Eq. (1) and obtain

$$\begin{bmatrix}\sigma_{xx}\\ \sigma_{yy}\\ \sigma_{zz}\\ \sigma_{zy}\\ \sigma_{zx}\\ \sigma_{xy}\end{bmatrix} = \begin{bmatrix}C_{11}\varepsilon_{xx}+C_{12}\varepsilon_{yy}+C_{13}\varepsilon_{zz}\\ C_{12}\varepsilon_{xx}+C_{11}\varepsilon_{yy}+C_{13}\varepsilon_{zz}\\ C_{13}\varepsilon_{xx}+C_{13}\varepsilon_{yy}+C_{33}\varepsilon_{zz}\\ 2C_{44}\varepsilon_{zy}\\ 2C_{44}\varepsilon_{zx}\\ 2C_{66}\varepsilon_{xy}\end{bmatrix} - \begin{bmatrix}e_{31}E_z\\ e_{31}E_z\\ e_{33}E_z\\ e_{15}E_y\\ e_{15}E_x\\ 0\end{bmatrix} - \begin{bmatrix}q_{31}H_z\\ q_{31}H_z\\ q_{33}H_z\\ q_{15}H_y\\ q_{15}H_x\\ 0\end{bmatrix}, \tag{A.1}$$

$$\begin{bmatrix}D_x\\ D_y\\ D_z\end{bmatrix} = \begin{bmatrix}2e_{31}\varepsilon_{zx}\\ 2e_{31}\varepsilon_{zy}\\ e_{31}\varepsilon_{xx}+e_{31}\varepsilon_{yy}+e_{33}\varepsilon_{zz}\end{bmatrix} + \begin{bmatrix}\kappa_{11}E_x\\ \kappa_{11}E_y\\ \kappa_{33}E_z\end{bmatrix} + \begin{bmatrix}\lambda_{11}H_x\\ \lambda_{11}H_y\\ \lambda_{33}H_z\end{bmatrix}, \tag{A.2}$$

$$\begin{bmatrix} B_x \\ B_y \\ B_z \end{bmatrix} = \begin{bmatrix} 2q_{31}\varepsilon_{zx} \\ 2q_{31}\varepsilon_{zy} \\ q_{31}\varepsilon_{xx} + q_{31}\varepsilon_{yy} + q_{33}\varepsilon_{zz} \end{bmatrix} + \begin{bmatrix} \lambda_{11}E_x \\ \lambda_{11}E_y \\ \lambda_{33}E_z \end{bmatrix} + \begin{bmatrix} \mu_{11}H_x \\ \mu_{11}H_y \\ \mu_{33}H_z \end{bmatrix}. \tag{A.3}$$

Let us consider the displacement, electric and magnetic fields are independent of fiber axis, $z-$ axis. That is,

$$u_j = u_j(x,y), \;\; E_j = E_j(x,y), \;\; H_j = H_j(x,y), \;\; j = x,y,z. \tag{A.4}$$

We have

$$\varepsilon_{zz} = 0, \;\; \varepsilon_{zy} = u_{z,y}, \;\; \varepsilon_{zx} = u_{z,x}. \tag{A.5}$$

With the above and the equilibrium equations (3), the problem splits naturally into the two problems

- Plane elasticity and transverse electromagnetic fields
  Constitutive laws:

$$\begin{bmatrix} \sigma_{xx} \\ \sigma_{yy} \\ \sigma_{xy} \\ D_z \\ B_z \end{bmatrix} = \begin{bmatrix} C_{11}\varepsilon_{xx} + C_{12}\varepsilon_{yy} \\ C_{12}\varepsilon_{xx} + C_{11}\varepsilon_{yy} \\ 2C_{66}\varepsilon_{xy} \\ e_{31}\varepsilon_{xx} + e_{31}\varepsilon_{yy} \\ q_{31}\varepsilon_{xx} + q_{31}\varepsilon_{yy} \end{bmatrix} + \begin{bmatrix} -e_{31}E_z \\ -e_{31}E_z \\ 0 \\ \kappa_{33}E_z \\ \lambda_{33}E_z \end{bmatrix} + \begin{bmatrix} -q_{31}H_z \\ -q_{31}H_z \\ 0 \\ \lambda_{33}H_z \\ \mu_{33}H_z \end{bmatrix}. \tag{A.6}$$

Equilibrium:

$$\begin{aligned} &\sigma_{xx,x} + \sigma_{xy,y} = 0, \\ &\sigma_{xy,x} + \sigma_{yy,y} = 0. \end{aligned} \tag{A.7}$$

- Anti-plane shear and in-plane electromagnetic fields
  Constitutive laws:

$$\begin{bmatrix} \sigma_{zx} \\ \sigma_{zy} \\ D_x \\ D_y \\ B_x \\ B_y \end{bmatrix} = \begin{bmatrix} 2C_{44}\varepsilon_{zx} \\ 2C_{44}\varepsilon_{zy} \\ e_{15}\varepsilon_{zx} \\ e_{15}\varepsilon_{zy} \\ q_{15}\varepsilon_{zx} \\ q_{15}\varepsilon_{zy} \end{bmatrix} + \begin{bmatrix} -e_{15}E_x \\ -e_{15}E_y \\ \kappa_{11}E_x \\ \kappa_{11}E_y \\ \lambda_{11}H_x \\ \lambda_{11}H_y \end{bmatrix} + \begin{bmatrix} -q_{15}H_x \\ -q_{15}H_y \\ \lambda_{11}H_x \\ \lambda_{11}H_y \\ \mu_{11}E_x \\ \mu_{11}E_y \end{bmatrix}. \tag{A.8}$$

Equilibrium:

$$\begin{aligned} &\sigma_{zx,x} + \sigma_{zy,y} = 0, \\ &D_{x,x} + D_{y,y} = 0, \\ &B_{x,x} + B_{y,y} = 0. \end{aligned} \tag{A.9}$$

References

Aboudi, J., 2001. Smart Mater. Struct. 10, 867.
Alshits, V.I., Darinskii, A.N., Lothe, J., 1992. Wave Motion 16, 265.
Arfken, G.B., Weber, H.J., 2001. Mathematical Methods for Physicists. Academic Press, San Diego.
Astrov, D.N. 1960. Sov. Phys.-JETP 11, 708.
Benveniste, Y., 1995. Phy. Rev. B 51, 16424.
Benveniste, Y., 1997. Mech. Mater. 25, 59.
Milton, G.W., 2001 The Theory of Composites, Cambridge University Press, Cambridge, (Chapter 6).
Berman, C.L., Greengard, L., 1994. J. Math. Phys. 35, 6036.
Bichurin, M.I., Petrov, V.M., Srinivasan, G., 2003. Phys. Rev. B 68, 054402.
Bichurin, M.I., Petrov, V.M., Ryabkov, O.V., Averkin, S.V., Srinivasan, G., 2005. Phys. Rev. B 72, 060408.
Camacho-Montes, H., Sabina, F.J., Bravo-Castillero, J., Guinovart-Díaz, R., Rodríguez-Ramos, R., 2009. Int. J. Eng. Sci. 47, 294.
Chen, T., 1993. J. Mech. Phys. Solids 41, 1781.
Chen, T., 1997. J. Mech. Phys. Solids 45, 385.
Eerenstein, W., Mathur, N.D., Scott, J.F., 2006. Nature 442, 759.
Fassi-Fehri, O., Hihi, A., Berveiller, M., 1989. Int. J. Eng. Sci. 27, 495.
Harshé, G., Dougherty, J.P., Newnham, R.E., 1993. Int. J. Appl. Electromagn. Mater. 4, 161.
Huang, J.H., 1998. Phys. Rev. B 58, 12.
Huang, J.H., Kuo, W.-S., 1997. J. Appl. Phys. 81, 1378.
Huang, H., Zhou, L.M., 2004. J. Phys. D: Appl. Phys. 37, 3361.
Kittel, C., 1986. Introduction to Solid State Physics. Wiley, New Jersey, pp. 8.
Kuo, H.-Y., Chen, T., 2007. Int. J. Eng. Sci. 45, 980.
Kuo, H.-Y., Chen, T., 2008. Int. J. Eng. Sci. 46, 1157.
Landau, L.D., Lifshitz, E.M., 1984. Electrodynamics of Continuous Media. Pergamon Press, New York, pp. 119.
Lee, J., Boyd IV, J.G., Lagoudas, D.C., 2005. Int. J. Eng. Sci. 43, 790.
Li, J.Y., Dunn, M.L., 1998a. Philos. Mag. A 77, 1341.
Li, J.Y., Dunn, M.L., 1998b. J. Intell. Mater. Syst. Struct. 9, 404.
Li, J.Y., 2000. Int. J. Eng. Sci. 37, 5579.
Li, Y.S., Duxbury, P.M., 1989. Phys. Rev. B 40, 4889.
Milgrom, M., 1997. J. Mech. Phys. Solids 45, 399.
Milgrom, M., Shtrikman, S., 1989. Phy. Rev. A 40, 1568.
Nan, C.-W., 1994. Phys. Rev. B 50, 6082.
Nan, C.-W., Bichurin, M.I., Dong, S., Viehland, D., Srinivasan, G., 2008. J. Appl. Phys. 103, 031101.
Nye, J.F., 1985. Physical Properties of Crystals. Clarendon Press, Oxford, pp. 300.
Perrins, D.R., McKenzie, D.R., McPhedran, R.C., 1979. Proc. Roy. Soc. Lond. A 369, 207.
Rado, G.T., Folen, V.J., 1961. Phys. Rev. Lett. 7, 310.
Rayleigh, L., 1892. Phil. Mag. 34, 481.
Ren, S.Q., Briber, R.M., Wuttig, M., 2008. Appl. Phys. Lett. 93, 173507.
Srinivas, S., Li, J.Y., Soh, A.K., Zhou, Y.C., 2006. J. Appl. Phys. 99, 043905.
Tang, T., Yu, W., 2008. Int. J. Eng. Sci. 46, 741.
Tang, T., Yu, W., 2009. Smart Mater. Struct. 18, 125026.
Li, S., 2000. Composites: Part A 32, 815.
Wu, T.-W., Huang, J.H., 2000. Int. J. Solids Struct. 37, 2981.
Zheng, Q.-S., Chen, T., 1999. Proc. R. Soc. Lond. A 455, 1301.